AFRL-SR-AR-TR-10-0011

REPORT DOCUMENTATION PAGE

1. REPORT DATE *(DD-MM-YYYY)*	2. REPORT TYPE	3. DATES COVERED *(From - To)*
02-28-2010	Final Performance Report	05/01/2007 - 11/30/2009

4. TITLE AND SUBTITLE	5a. CONTRACT NUMBER
Computational Electromagnetics application to small geometric anomalies and associated uncertainty evaluation	FA9550-07-1-0436

5b. GRANT NUMBER

5c. PROGRAM ELEMENT NUMBER

6. AUTHOR(S)	5d. PROJECT NUMBER
Akash Anand and Oscar P. Bruno	

5e. TASK NUMBER

5f. WORK UNIT NUMBER

7. PERFORMING ORGANIZATION NAME(S) AND ADDRESS(ES)	8. PERFORMING ORGANIZATION REPORT NUMBER
Mathematical Systems & Solutions, Inc. 685 Busch Garden Dr Pasadena, CA 91105	

9. SPONSORING/MONITORING AGENCY NAME(S) AND ADDRESS(ES)	10. SPONSOR/MONITOR'S ACRONYM(S)
AF OFFICE OF SCIENTIFIC RESEARCH 875 N. RANDOLPH ST. ROOM 3112 ARLINGTON VA 22203 NA	11. SPONSOR/MONITOR'S REPORT NUMBER(S)

12. DISTRIBUTION/AVAILABILITY STATEMENT

Distribution A: Approved for Public Release

20100329199

13. SUPPLEMENTARY NOTES

14. ABSTRACT

The work performed under this effort has resulted in development of variety of important
computational electromagnetics tools enabling efficient application to problems involving
small geometric anomalies and associated uncertainty evaluation, including
1. Issues related to highly efficient implementations of integral EM approaches suitable
for extension to high-performance parallel solvers;
2. Surface repair and representation of openings and surface variabilities and methodologies
for surface repair of highly-damaged or highly-inaccurate geometry representations;
3. Consideration of issues related to uncertainty quanti
cation for both continuous and discrete random variables, with special attention to the
context of EMC/EMI, and development of adaptive stochastic collocation and reduced order

15. SUBJECT TERMS

Computational electromagnetics.

16. SECURITY CLASSIFICATION OF:			17. LIMITATION OF ABSTRACT	18. NUMBER OF PAGES	19a. NAME OF RESPONSIBLE PERSON
a. REPORT	b. ABSTRACT	c. THIS PAGE	NONE	15	Marta B. Kahl
Unclassified	Unclassified	Unclassified			19b. TELEPHONE NUMBER *(Include area code)* 626-818-8642

"Computational Electromagnetics application to small geometric anomalies and associated uncertainty evaluation"

Final Report

Performance period: May 1st 2007 - November 30th 2009

Mathematical Systems & Solutions Inc.
685 Busch Garden Dr., Pasadena, CA 91105

Objectives

The present effort seeks development of efficient algorithms for evaluation of leakage of electromagnetic scattering through openings in context in which significant uncertainty may exist. Our effort addresses this main objective through three main complementary goals, namely: 1) Development of fast and accurate solvers for electromagnetic scattering by *open* surfaces containing edges, corners and other geometric singularities; 2) Accurate representation of surfaces, with particular emphasis on surface anomalies, openings and random surface features; and, for problems including surface imperfections and/or other random geometric features 3) Appropriate methods enabling uncertainty quantification and evaluation of random effects. In November 2007 a new task was added to this list, namely, 4) Modelling of the scattering and radiation properties of wire antennas. The CEM software resulting from this work should enable effective evaluation of leaking fields for complex structures of interest to the Air Force, for all frequencies arising in relevant applications.
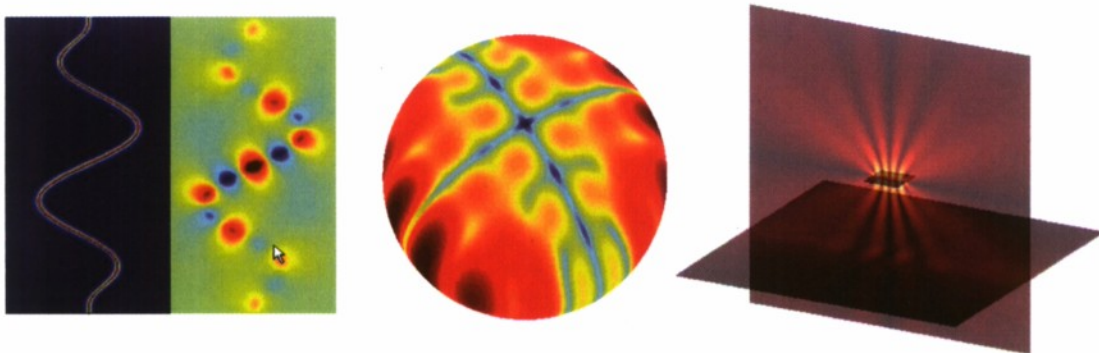

Figure 1: Propagation and scattering problems enabled by the new methodologies.

Status of Effort

The work performed under this effort has resulted in development of variety of important computational-electromagnetics tools enabling efficient application to problems involving small geometric anomalies and associated uncertainty evaluation, including
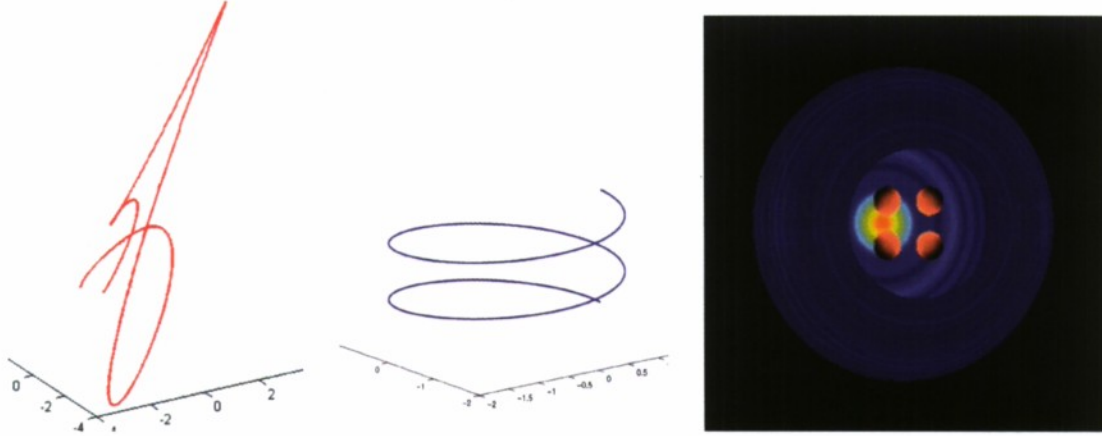
Figure 2: Left and Center: Curved wire antennas considered in our development of wire antenna solvers. Right: Fields leaked through an opening in a body containing a small interior structure.

1. Issues related to highly efficient implementations of integral EM approaches suitable for extension to high-performance parallel solvers;

2. Surface repair and representation of openings and surface variabilities and methodologies for surface repair of highly-damaged or highly-inaccurate geometry representations;

3. Consideration of issues related to uncertainty quantification for both continuous and discrete random variables, with special attention to the context of EMC/EMI, and development of adaptive stochastic collocation and reduced order modelling methods; and

4. Development of integral-equation solvers for *electromagnetic* scattering by wire antennas and open surfaces, with attention to solution singularities, pseudo-differential character of the integral operators, and associated spectral distributions and required numbers of GMRES iterations.

Our results in these areas is described in what follows.

Electromagnetic scattering from open surfaces: Mathematical Formulation

In view of the normal and tangential singularities of surface currents for open surfaces, we seek the scattered electric field off an open Perfect Electrically Conducting (PEC) surface Γ in the form

$$\mathbf{E}^s(z) = ik \int_\Gamma G_k(|z - y|) W\mathbf{I}(y) ds(y) + \frac{i}{k} \nabla \int_\Gamma G_k(|z - y|) \mathrm{div}_\Gamma(W\mathbf{I}) ds(y), \qquad (1)$$

where W is a "weight" matrix and where, denoting by $\mathbf{J}$ the actual surface current and letting $\mathbf{J} = W\mathbf{I}$ ($\mathbf{I}$ is a "regularized" bounded surface current and W carries explicitly the

2

current singularity at the edge), the regularized current I satisfies the EFIE equation

$$\mathcal{T}_W \mathbf{I} = -\mathbf{n} \times \mathbf{E}^{inc}. \tag{2}$$

Here $\mathbf{n}$ is the normal to Γ. The weighted integral operator can be written as

$$\mathcal{T}_W \mathbf{I} = \mathcal{S}_W \mathbf{I} + \mathcal{D}_W \mathbf{I} \tag{3}$$

where operators $\mathcal{S}_W$ and $\mathcal{D}_W$ are defined as

$$\mathcal{S}_W \mathbf{I} = ik\mathbf{n} \times \int_\Gamma G_k(|x - y|) W \mathbf{I}(y) ds(y) \tag{4}$$

and

$$\mathcal{D}_W \mathbf{I} = -\frac{i}{k} \overrightarrow{\text{curl}}_\Gamma \int_\Gamma G_k(|x - y|) \text{div}_\Gamma (W\mathbf{I}) ds(y) \tag{5}$$

respectively. Here, for a scalar field F defined on the surface Γ, $\overrightarrow{\text{curl}}_\Gamma$ denotes the operator

$\overrightarrow{\text{curl}}_\Gamma F = (\nabla F) \times \mathbf{n}.$

Let $\vec{r}(u, v)$ be a local coordinate chart with $(u, v) \in (0, 1) \times (0, 1)$ such that $v = 0$ correspond to an open edge. In this case, the unknown density $\mathbf{I}$ can be decomposed as

$$\mathbf{I} = I^u \vec{r}_u + I^v \vec{r}_v$$

where I^u and I^v are the tangential and normal components of the surface current. Given that the tangent and normal components of the solution have singularity of $O(1/\sqrt{d})$ and $O(\sqrt{d})$ respectively, where d denotes the distance to the edge, the choice of weight matrix

$$W = \frac{1}{\omega} \begin{pmatrix} 1 & -\theta\omega^2 \\ 0 & \omega^2 \end{pmatrix} \tag{6}$$

with $\omega \sim \sqrt{d}$, and $\theta = \vec{r}_u \cdot \vec{r}_v / \vec{r}_u \cdot \vec{r}_u$, that act on tangential and normal components $(I^u, I^v)^T$ of $\mathbf{I}$ as a multiplication by the matrix renders I^u and I^v smooth.

Before we discuss the numerical method that is used of to solve (2), we note that once the surface current density J is obtained as a solution of (2), the electric field can be retrieved using equation (1). Also, if we define the electric far field $\mathbf{E}_\infty(\hat{x})$ as

$$\mathbf{E}^s(x) = \frac{e^{ik|x|}}{|x|} (\mathbf{E}_\infty(\hat{x}) + \mathcal{O}(|x|^{-1})) \tag{7}$$

then, one can use the expression

$$\mathbf{E}_\infty(x) = \frac{ik}{4\pi} \hat{x} \times \int_\Gamma e^{-ik\hat{x} \cdot y} (W\mathbf{I}(y) \times \hat{x}) ds(y) \tag{8}$$
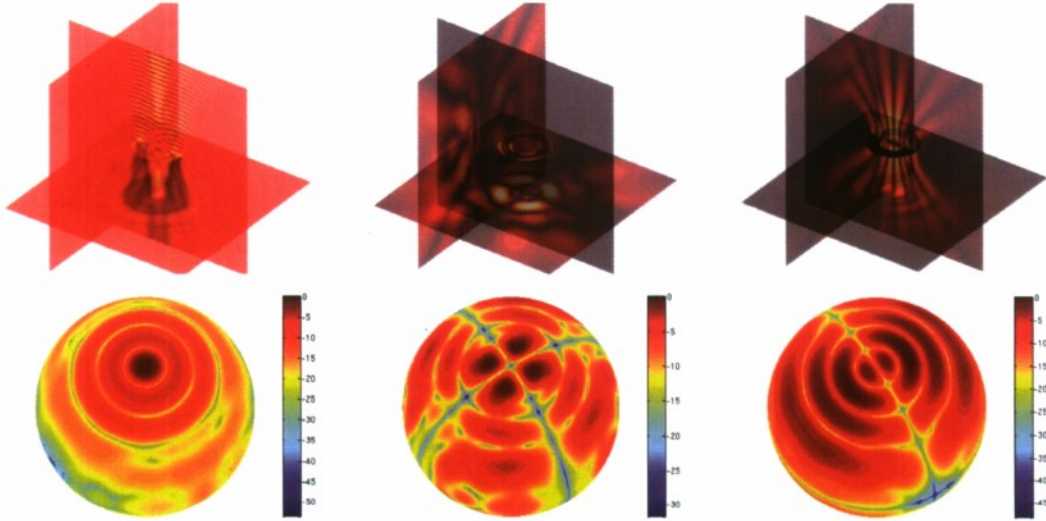
3

Figure 3: Electromagnetic scattering of an x-polarized incident plane wave of $k = 16$ from an annulus. Top row, left, center and right show x, y and z components of the total field near the scatterer whereas bottom row shows corresponding far fields in dB, normalized to the maximum.

for the electric far field computation.

Scatterers with corners

The presence of corners in a scattering geometry results in solutions that become unbounded where this blow-up is of different nature from that at open edges. It, thus, poses a significant challange for the numerical scheme described above in term of achieving high accuracy. In view of this, we adopt a strategy where we solve "nearby" problems on smooth domains that coincide with the original scatterer except in small neigborhoods near the corner. The success of the strategy hinges on its ability to use extremely close approximations of the domains with corners and use of discretization that give rise to solution with limited computational cost. Here, corners have been smoothed via a systematic blending of two arcs on either side of the corner. In the following discussion, we describe the procedure that we adopt to smoothly round these corners. *We emphasize that the procedure is completely general and automatic: it can be applied with ease to a general open surface, with curved edges and associated corners.*
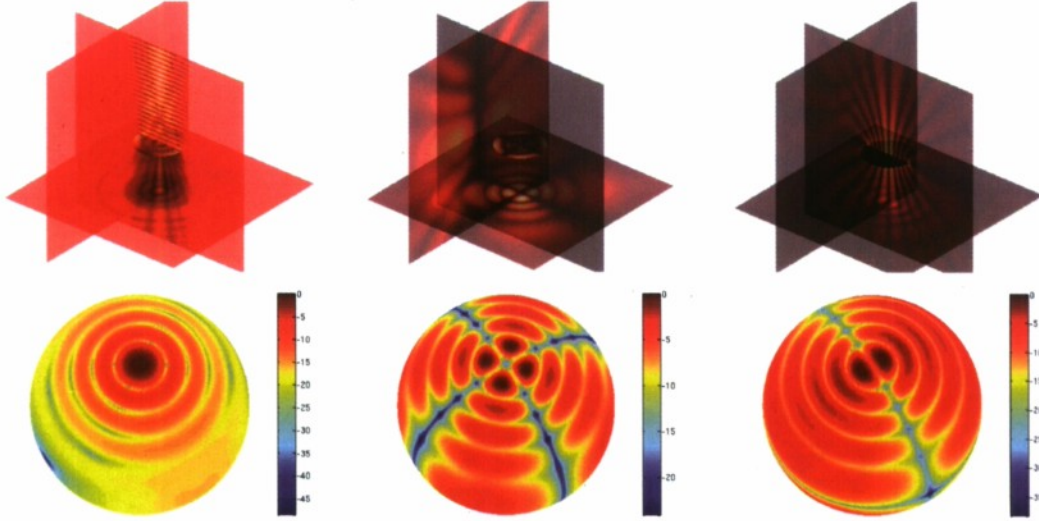
4

Figure 4: Electromagnetic scattering of an x-polarized incident plane wave of $k = 16$ from a unit disc. Top row, left, center and right show x, y and z components of the total field near the scatterer whereas bottom row shows corresponding far fields in dB, normalized to the maximum.

Preconditioned Equations

In order to solve better conditioned integral equations, we precondition equation (2) on the left by means of the regularizing operator $\mathcal{T}_\omega$ defined by

$$
\mathcal{T}_\omega \mathbf{K} = ikn \times \int_\Gamma G_k(|x - y|)W\mathbf{K}(y)ds(y)
$$

$$
- \frac{i}{k}\overrightarrow{\mathrm{curl}}_\Gamma \int_\Gamma G_k(|x - y|)\omega(y)\mathrm{div}_\Gamma(\mathbf{K})ds(y)
$$

$$
= \mathcal{S}_W\mathbf{K} + \mathcal{D}_\omega\mathbf{K}. \tag{9}
$$

More precisely, we will solve

$$
\mathcal{T}_\omega \circ \mathcal{T}_W(\mathbf{I}) = -\mathcal{T}_\omega(\mathbf{n} \times \mathbf{E}^{inc}) \tag{10}
$$

where we express the operator on the left-hand side as

$$
\mathcal{T}_\omega \circ \mathcal{T}_W = \mathcal{S}_W \circ \mathcal{S}_W + \mathcal{S}_W \circ \mathcal{D}_W + \mathcal{D}_\omega \circ \mathcal{S}_W. \tag{11}
$$

We note that the operator $\mathcal{D}_\omega$ can be evaluated in a straightforward manner using differentiation and integration methods described in the previous section.

Numerical implementation

In this section, we present the main algorithmic components of the numerical scheme that we employ in solving (2), which in turn reduces to accurate evaluations of the weighted integral operator $\mathcal{T}_W$ and hence S_W and D_W.
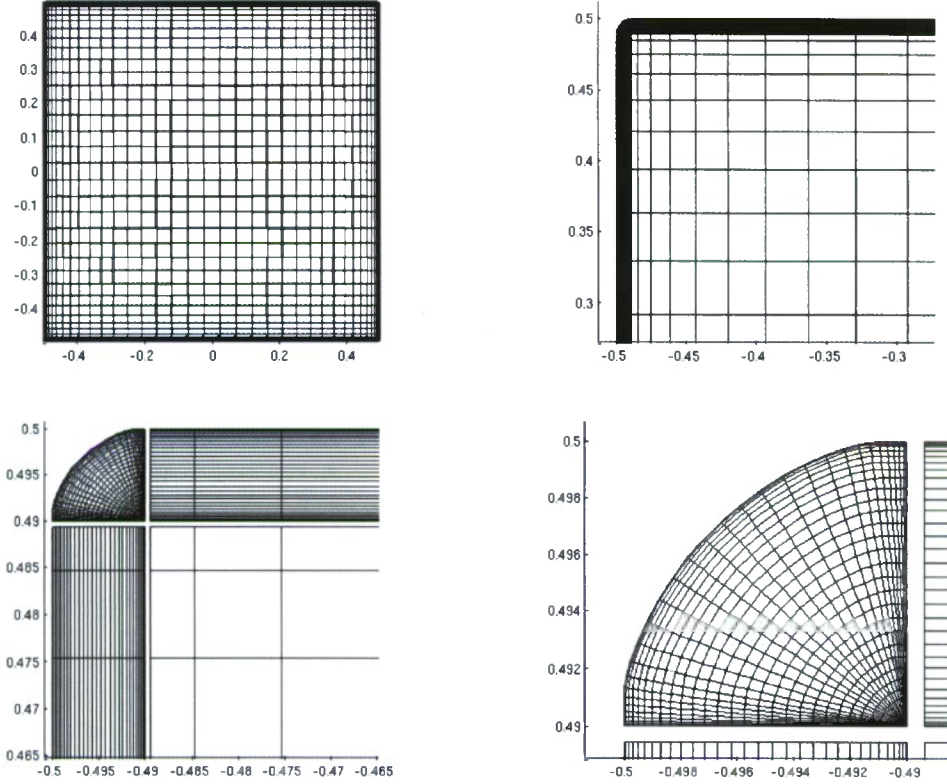
5

Figure 5: A unit square with smoothly rounded corners. The geometry is divided into interior, edge and corner patches and are discretized as shown above.

We note that the accurate evaluation of $\mathcal{S}_W$ in (4) entails obtaining $(I^u, I^v)^T$ from **I**, which is quite straightforward. An application of the W-matrix on $(I^u, I^v)^T$ leads to integrals of the form

$$S_\omega[\phi](x) = \int_\Gamma \frac{1}{\omega} G_k(|x - y|)\phi(y)ds(y), \tag{12}$$

where ϕ is smooth, that can then be approximated through a specialized numerical integration method. Toward this end, we employ a high order quadrature that relies on a smooth cut-off function η_x supported in a small neighborhood of the target point x that is also identically equal to one, i.e., $\eta_x \equiv 1$, in the immediate neighborhood of x, to split (12) as

$$S_\omega[\phi](x) = \int_{\eta_x \neq 0} \frac{1}{\omega} G_k(|x - y|)\eta_x(y)\phi(y)ds(y) + \int_\Gamma \frac{1}{\omega} G_k(|x - y|)(1 - \eta_x(y))\phi(y)ds(y). \tag{13}$$

Clearly, the second integral in (13) can be accurately approximated using a "Weighted
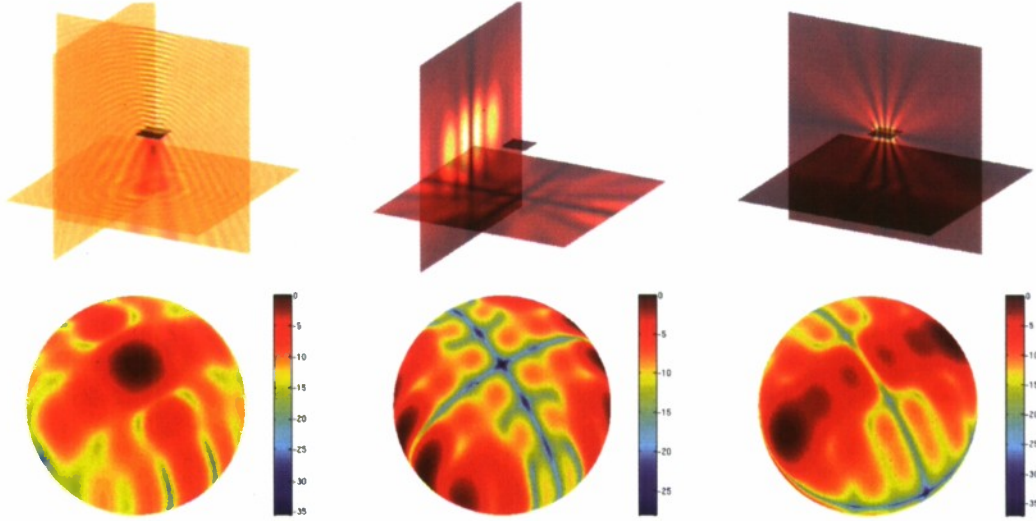
Figure 6: Electromagnetic scattering of an x-polarized incident plane wave of $k = 16$ from a square plate. Top row, left, center and right show x, y and z components of the total field near the scatterer whereas bottom row shows corresponding far fields in dB, normalized to the maximum.
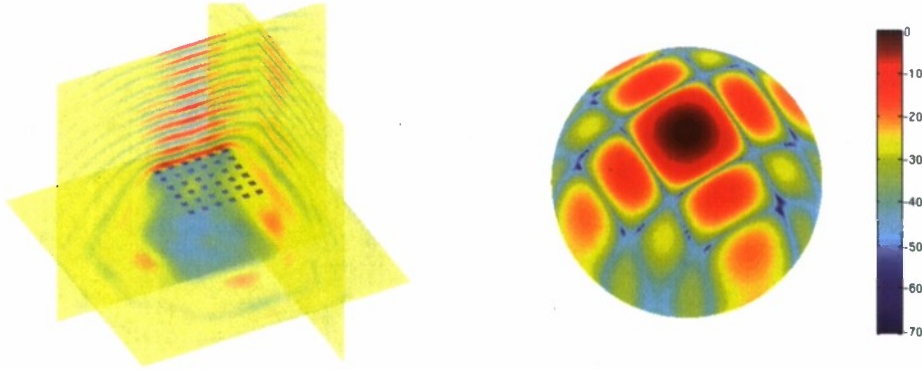

Figure 7: Scalar case: Scattering of a normally incident plane wave of wavelength 8.4 mm from a 6 by 6 array of square plates of dimensions 2 by 2 mm. In this example, we allowed a random variation in dimensions and locations of plates on the scale of microns. Left : The field near the array is shown. Right : Corresponding far field in dB, normalized to the maximum.

Clenshaw-Curtis" quadrature of the form

$$\int_0^1 \frac{1}{\sqrt{v}} f(v) dv \approx \sum_{n=0}^{N} w_n f(v_n), \tag{14}$$

where the quadrature points are given by

$$v_n = \frac{1}{2}\left(1 + \cos\left(\left(n + \frac{1}{2}\right)\frac{\pi}{N}\right)\right)$$

and quadrature weights, w_n, by

$$w_n = \frac{1}{N}\sum_{m=0}^{N}{}' -\frac{4}{4m^2 - 1}\cos\left(\left(n + \frac{1}{2}\right)\frac{m\pi}{N}\right)$$

where the primed sum denotes that the first term ($m = 0$) is halved. The first integral in (13), on the other hand, is evaluated by changing to polar coordinates, where ρ-integrals are performed using a scaled version of (14) and θ-integral is evaluated using regular Clenshaw-Curtis quadrature for each piecewise smooth θ-interval.

In the evaluation of D_W in (5), however, care should be taken when dealing with the term $\mathrm{div}_\Gamma(W\mathbf{I})$ so that the singular weight ω gets proper treatment. To this end, we use the formula for the surface divergence in coordinates. For this, we use the fact that for a given tangential field $\mathbf{X} = X^u\vec{r}_u + X^v\vec{r}_v$ on the patch $\vec{r}(u,v)$, the formula for the tangential divergence reads:

$$\mathrm{div}_\Gamma\mathbf{X} = \frac{1}{\sqrt{g}}[\partial_u(\sqrt{g}X^u) + \partial_v(\sqrt{g}X^v)] \tag{15}$$

where $g = EG - F^2$ is the Riemannian metric tensor, with $E = \vec{r}_u \cdot \vec{r}_u$, $F = \vec{r}_u \cdot \vec{r}_v$ and $G = \vec{r}_v \cdot \vec{r}_v$. A straightforward application of (15) thus yields

$$\begin{aligned}
\mathrm{div}_\Gamma(W\mathbf{I}) &= \frac{1}{\omega}\left[\frac{1}{2g}\left(\partial_u g(I^u - \theta\omega^2 I^v) + \partial_v g\,\omega^2 I^v\right)\right.\\[2ex]
&\quad\left. + \partial_u I^u - \partial_u\theta\omega^2 I^v - \theta\omega^2\partial_u I^v + \omega^2\partial_v I^v + \frac{1}{2}\partial_v(\omega^2)I^v\right]
\end{aligned} \tag{16}$$

assuming that ω depends only on v. From the expression in (16), it follows that the integral

$$\int_\Gamma G_k(|x - y|)\mathrm{div}_\Gamma(W\mathbf{I})ds(y)$$

in (5) has the same form as in (12) and thus can be evaluated using the integration scheme described above.

The last remaining element of our numerical algorithm pertains to derivative computations that arise in (16) as well as in the surface curl differential operator in (5). As these

expressions only involve partial derivatives of smooth functions, one can use Chebyshev polynomials as spectrally accurate functional approximations, which can then be used for finite difference approximation of the derivatives of these functions. One can also directly differentiate the approximating Chebyshev series to obtain necessary derivatives. In this case, the loss of accuracy near patch edges can be controlled by restricting the degree of Chebyshev polynomials to a moderate number.

Numerical Experiments

In this section we report on a variety of numerical experiments we have conducted to demonstrate the solvers developed under the present effort, for both scalar and vector electromagnetic cases, and from various scattering configurations. We start by presenting two examples of electromagnetic wave scattering from an annulus in Figure 3 and from a unit disc in Figure 4. One critical difference between these simulations and similar ones we considered in previous methods is the use of non-overlaping patches for the description of the scattering geometry. The use of non-overlapping patches, even though not essential for annulus and disc geometries, is the backbone of our technology required for scattering simulations from geometries with corners. For these singular geometries, we adopt the corner smoothing described above Section. An electromagnetic wave scattering from a "sharply-smoothed" square plate, that coincide with the original scatterer except in small neighborhoods near the corner (and essentially equals the sharp square plate), is presented in Figure 6. We also include some results for scalar wave scattering where the scattering geometry mimics a small scale array of size 6 by 6 in Figure 7. Figures 2 right and 8, finally, depict solutions of problems involving leakage of energy through holes, and the interaction of leaked energy with scattering elements.

Enhancement and Extension of Geometry Representation Software

Significant enhancements were introduced to the geometry representation capability, enabling treatment of heavily damaged structures. The new capabilities are demonstrated in Figures 10 and 11. Clearly, the new software can be used to repair surfaces containing very challenging features, including very coarse, low quality discretizations, detachment, lack of water-tightness, etc.

Curved wire antenna solvers

We developed an extension of the methodology previously put forward in collaboration with M. Haslam for straight wire antennas ("Regularity theory and super-algebraic solvers for wire antenna problems", O. Bruno and M. C. Haslam; SIAM Jour. Sci. Comp. **29** 1375–1402. (2007)) that applies to arbitrary curved wire antennas. The resulting code is applicable to arbitrary closed or open curved wires (such as those shown in Figure 2) driven by an incident field. The present curved wire code is based on use of the electric field integral equation with a thin-wire approximation—according to which the electrical current J is constant around the circular cross-section that results as the wire is cut by an orthogonal plane. This approximation is commonly used in the literature; for example we mention the contributions provided by Wu (1962) for a circular geometry, as well as
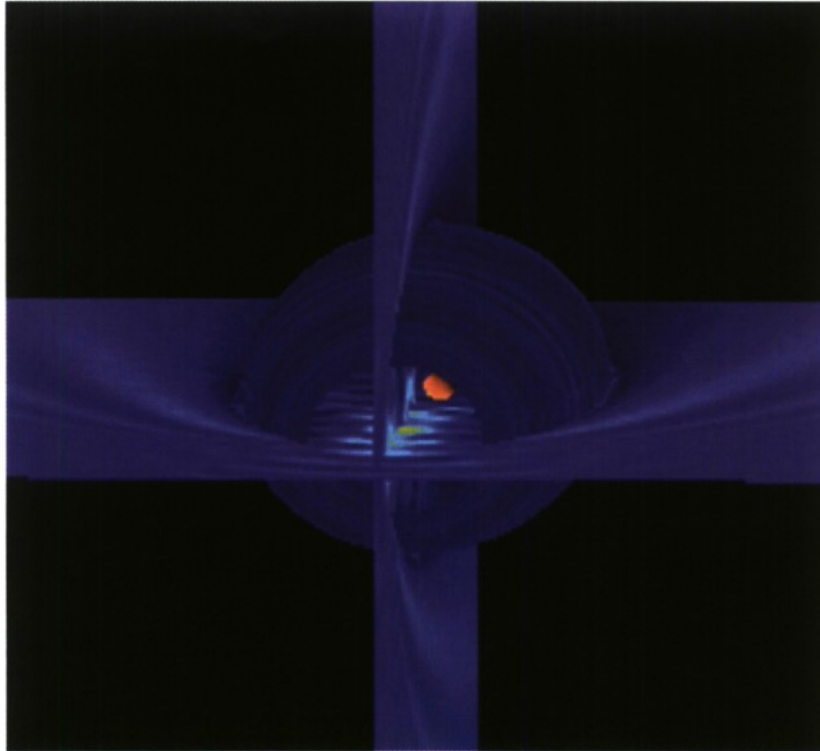
Figure 8: Leakage: Scalar fields within and around a body containing a an opening and a small interior structure.

the recent article by Champagne and Wilton (2006). (The latter paper incorporates high-order elements; however, since the logarithmic singularity is treated using a tangent line approximation the approximation is reduced to lowest order.) We believe our algorithm is the first one to deliver high-order accuracy for the curved-wire problem. Our code is able to solve highly challenging wire-scattering problems. For example, interactions with RPIs Prof. Margaret Cheney and AFRL's Dr. Matthew Ferrara resulted in solutions for a very challenging problem concerning a wire 600λ in length. Solutions with eight digits of accuracy were obtained for this problem in a computational time of the order of ten minutes in a single processor computer. We were told by Dr. Ferrara that commercial software they use requires inordinately long computing times to produce any sort of approximate solution for this problem.

Uncertainty quantification for EMC/EMI applications

We have developed and implemented a fast method to enable the statistical characterization of electromagnetic interference and compatibility (EMI/EMC) phenomena on electrically large and geometrically complex targets. The main goal is to demonstrate the ability to accurately and robust characterize the impact of uncertainty in electromagnetic excitations and/or system geometry and configuration on electrical components. The focus has been on problems related to aircraft safety.

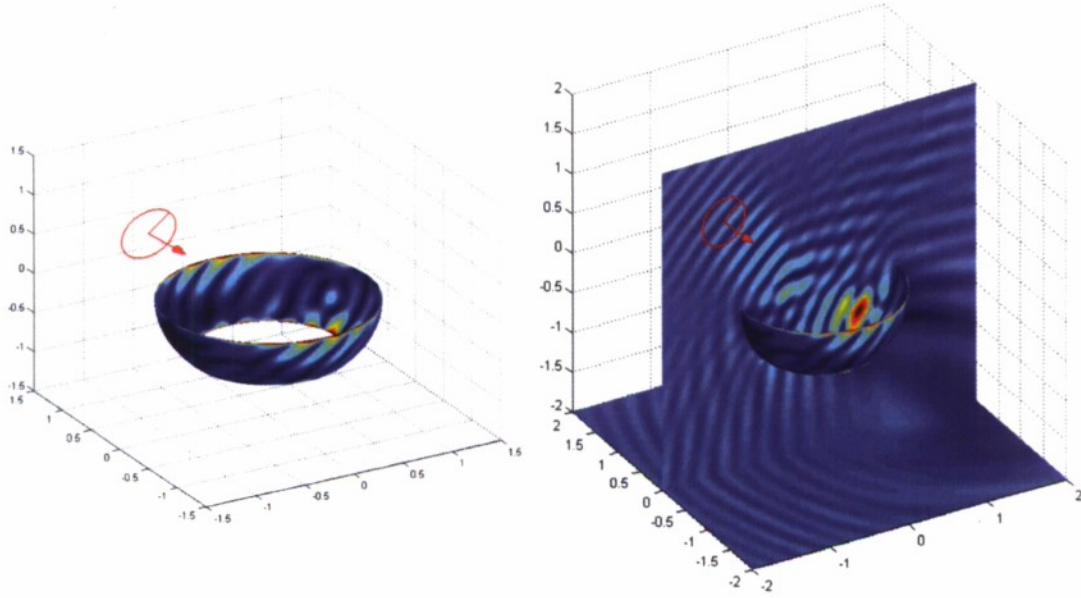The system uncertainty is parameterized in terms of a, potentially high, number of ran-

Figure 9: Left: model open surface scatterer: annulus; note the arrow indicating the propagation direction of the incident field, and the radius indicating the polarization, that is, the orientation of the electric field vector. Right: resulting current on the annulus. Note that, in spite of the symmetry of the incidence, the current is not circularly symmetric—as a result of the electrical polarization.

dom variables. The dimensionality of the system is estimated based on prior knowledge of the problems, e.g., number of wires or dimensional estimation through spatial correlations for materials or geometries, and the type of the random variables are chosen to most accurately reflect the prior knowledge. In the problems we have consider both normal and beta-distributed random variables.

After parametrization, the uncertainty is addressed through a polynomial chaos representation and a stochastic collocation procedure, requiring the solution of a number of problems for specific parameter choices. We used a fast time-domain solver for this but alternatives are equally useful. The collocation approach is based on Stroud sparse integration methods, which require only 2d+1 samples for a d-dimensional problem while yielding reasonable accuracy. The saving over a standard Monte Carlo method is dramatic. Outputs of interests are then computed by processing the particular solutions to compute mean and variances for measures of interest, e.g., induced currents.

As an example of demonstrated capability and practicality of the approach, consider an airplane cockpit (Figure 12), which is illuminated by a plane wave at a random angle. The source induces currents on cables and shielded PC cards and one wishes to statistically characterize these current under the uncertainty of the source location, cable positions and cable loads. The general setup is illustrated below. We use 17 uniformly distributed variables to represents the location of cables, direction of plane wave source and load resistors in the shielded PC boxes. In Figure 13 we illustrate the computed current at a terminal as well as the sensitivity of the current over a frequency range of the source. This technique has been carefully validated against direct Monte Carlo modeling for simpler tests, showing excellent agreement at a dramatically reduced computational cost.
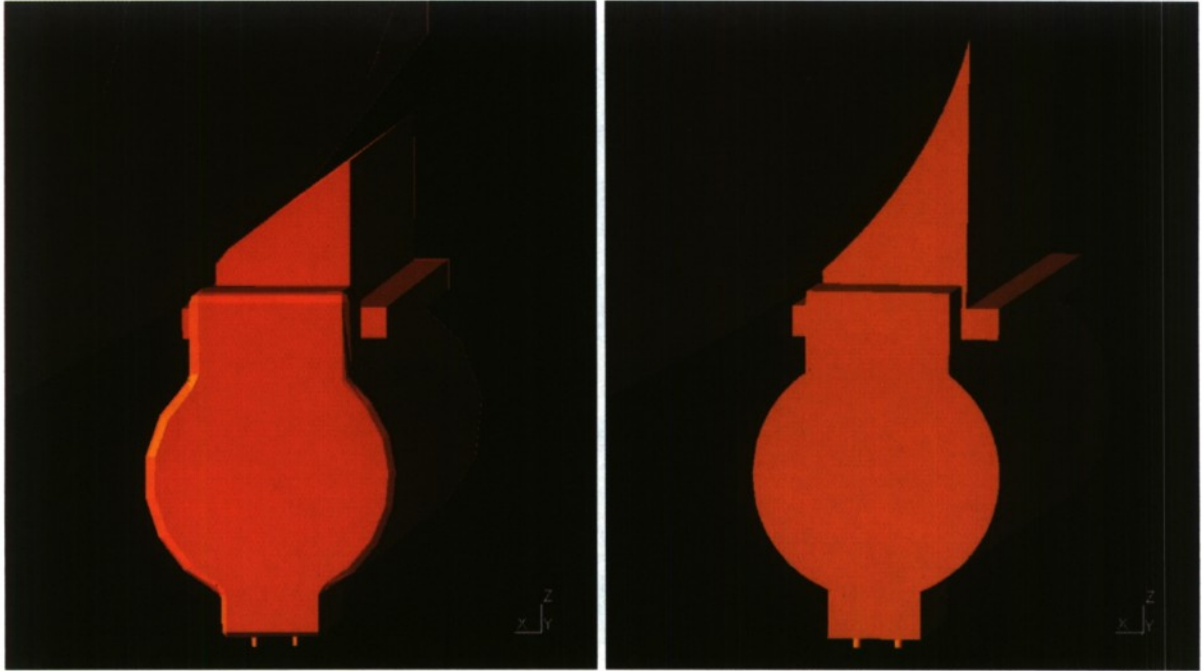
11

Figure 10: Detached and re-attached pylon, front view. Left: Original low quality surface rendering. Right: processed surface by means of the continuation method surface representation algorithm.

We are currently exploring the extension of these techniques to discrete random variables to enable the modeling of holes and cracks along with the other types of uncertainty already discussed in the above.

Adaptive stochastic collocation methods

In the example above, we used Stroud based integration techniques to enable the modeling of high-dimensional problems. While these often are successful, there are more complex problems where higher accuracy is needed, e.g., to compute higher moment statistics.

To address this problem, we have developed adaptive stochastic collocation methods. These are based on the Smolyak construction of high-dimensional sparse grids in combination with the lesser-known hierarchical Gauss-Patterson integration rules. The hierarchical nature of the integration points along with the Gauss-like accuracy (3/2N exactness vs 2N for Gauss) enables a dramatically reduced overall cost for a given accuracy. This is illustrated in Figure 14 where we show the time vs accuracy curve for three integration formulas Gauss quadrature, Gauss-Patterson, and Clenslaw-Curties the latter one is the standard use in most existing Smolyak based integration methods.

The results in Figure 14 are for one-dimensional functions but the benefits in higher dimensional problems are even more striking due to the hierarchical nature of the quadrature points. For example, in a three-dimensional space, the number of points for Clenshaw-Curtis and Gauss-Patterson rules are about the same for a given level of refinement, however, as we see above, the accuracy is considerably better for the latter case. The number of quadrature points for the Gauss-based approach is twice that, i.e., for a similar accuracy, the work has
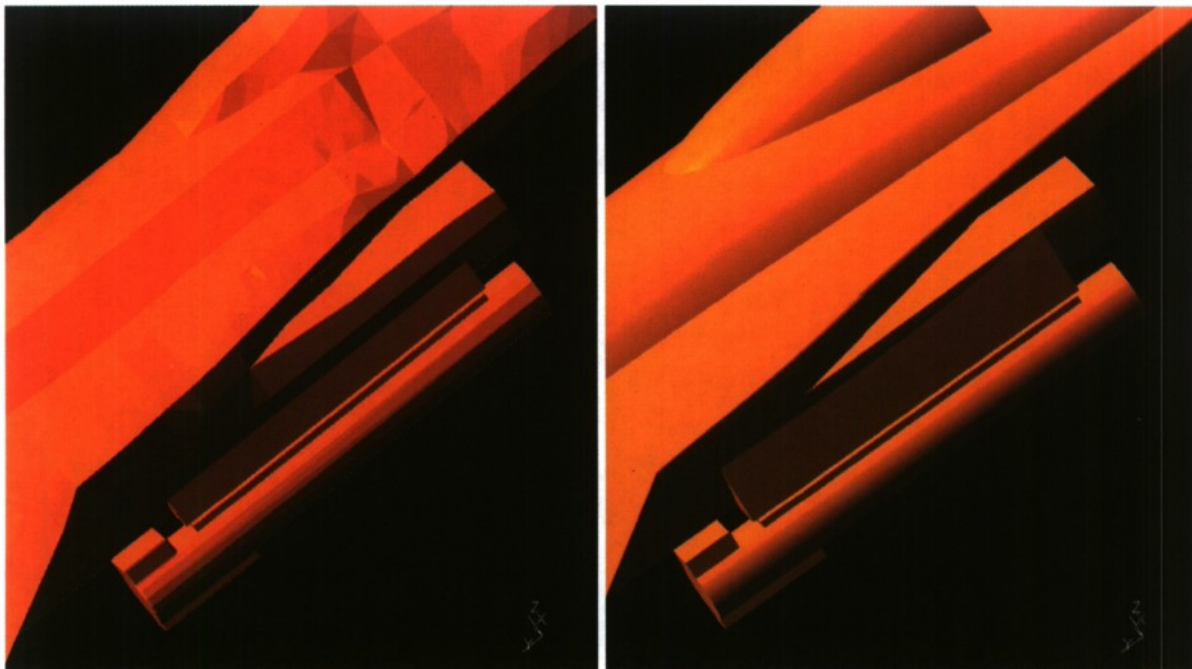
Figure 11: Side view. Left: Original low quality surface rendering. Right: processed surface by means of the continuation method surface representation algorithm.

been reduced by 50%.

The hierarchical nature of the Gauss-Patterson rules offers another benefit at limited cost an embedded error estimator since at any level we can also look back and compute statistical measures at a lower formal accuracy and compare to estimate accuracy.

We have developed in a dimension-by-dimension approach in which the Smolyak sparse grid develops and refines only on those dimensions where the error estimator indicates significant activity. This not also reduces the computational cost but also offers valuable insight into the strength of parameter-space coupling.

This has been successfully tested on high-dimensional dynamical systems, leading to substantial computational savings, and we are currently exploring the use of such techniques for electromagnetic scattering problems and extensions to discrete variables.

Reduced order modeling for uncertainty quantification

A final major effort concerning uncertainty quantification has been devoted to the ongoing development of methods of reduced computational complexity to further limit the cost of sampling in high-dimensional parameter space. This has been successfully demonstrated for parametrized Maxwells equations on differential form and we have recently begun the development of such techniques for methods based on integral equations and boundary element methods.

The computational and theoretical bottleneck in these based is the development of a rigorous a posteriori error-theory. This is, however, essential for validate the accuracy of the reduced complexity model and is also used in a greedy approach in the construction of
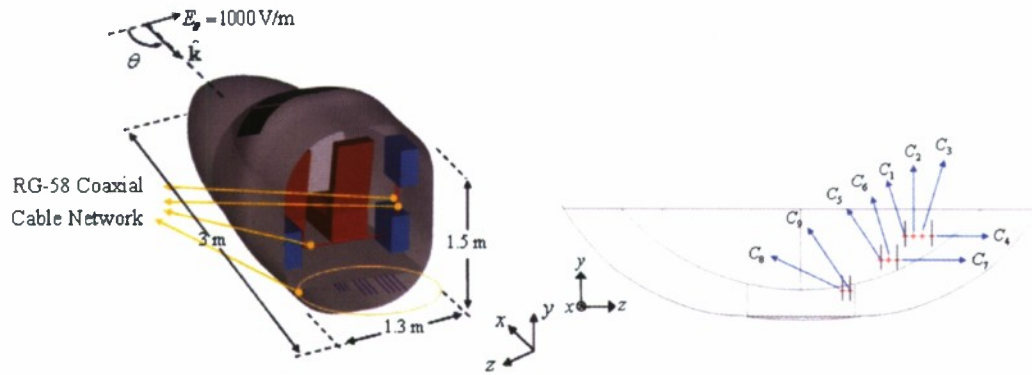
Figure 12: On the left is shown the general cockpit layout with source and shielded PC boxes for EMI/EMC computation. On the right is illustrated the location of the cables under the cockpit floor. The locations of these are all uncertain.
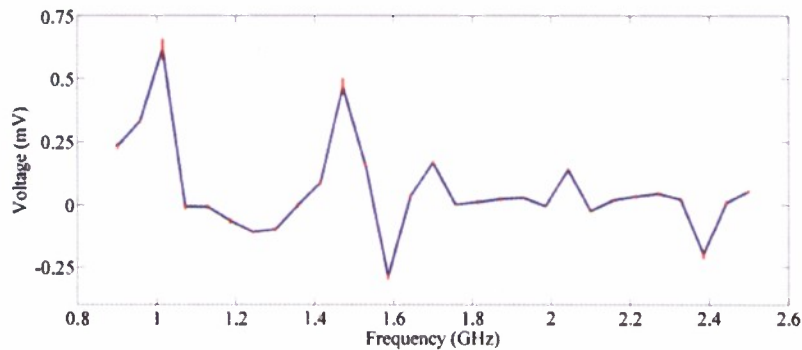

Figure 13: Computed current at a terminal as well as the sensitivity of the current over a frequency range of the source.

the reduced model.

This work is still ongoing for general cases and integral equation based models and we hope to report on more details and results during the coming year.

Personnel Associated with the Research Effort

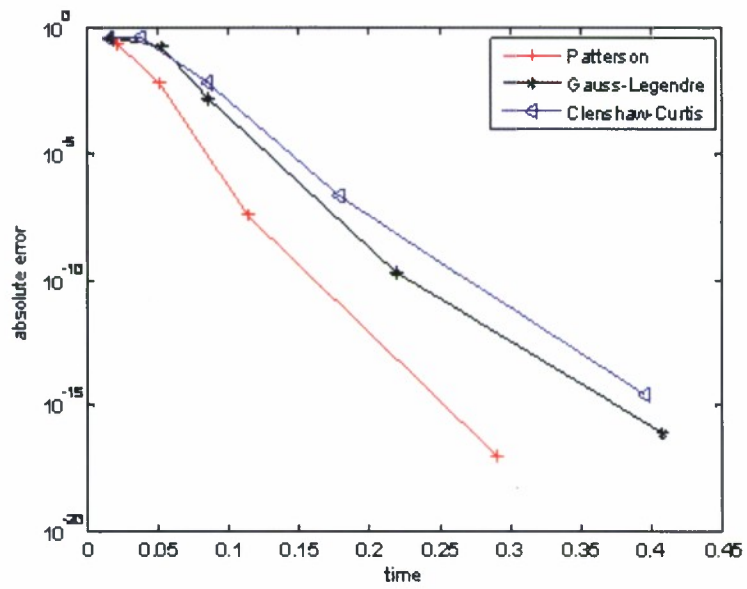A. Anand, O. Bruno, J. Hesthaven, J. Huh.

Figure 14: Cost vs accuracy for different integration formulas, highlighting the importance of using the Gauss-Patterson approach.